Int. J. Heat Mass Transfer. Vol. 34, No. 6, pp. 1491–1502, 1991
Printed in Great Britain

0017–9310/91 $3.00 + 0.00

An enthalpy formulation for phase change problems with a large thermal diffusivity jump across the interface

S. L. LEE and R. Y. TZONG

Department of Power Mechanical Engineering, National Tsing-Hua University, Hsinchu, Taiwan 30043, Republic of China

(*Received* 3 *October* 1989 *and in final form* 12 *July* 1990)

Abstract—An enthalpy formulation is proposed in the present investigation for a phase change material (PCM) having a distinct freezing temperature. The latent heat is separated from the sensible heat such that there exists a dependent variable (the sensible heat) that is a continuous function over the entire physical domain. Inside each control volume, the latent heat is rigorously evaluated from the fraction of the liquid phase to achieve an even latent heat evolution. In the dimensionless transformation, the characteristic time is defined in terms of the Stefan number. The coefficients of the unsteady terms thus are always less than unity. This will achieve a good numerical stability for any Stefan number. In addition, this particular transformation makes the present enthalpy formulation applicable to single phase problems if an infinite Stefan number is assigned. To account for a thermal diffusivity jump at the liquid–solid interface, a modified weighting function scheme is developed. Through a few examples, the present enthalpy formulation is seen to produce an accurate and smooth liquid–solid interface for PCM having a distinct freezing point.

INTRODUCTION

THE ENTHALPY formulation has been widely used in solving phase change problems, because there is no need to track the movement of the liquid–solid interface during the melting or solidification process. However, for a phase change material (PCM) having a distinct freezing point, an enthalpy discontinuity exists at the liquid–solid interface. This phenomenon causes a serious numerical instability in the use of enthalpy formulation. To circumvent this difficulty, most previous investigators assumed a phase change taking place over a range of temperatures such that a continuous variation of enthalpy can be constructed across the artificial 'mushy zone'. Unfortunately, such a treatment might have an appreciable influence on the results as pointed out by Bonacina *et al.* [1].

To remove the need of an artificial mushy zone, Shamsundar and Sparrow [2] proposed an enthalpy model in conjunction with an implicit finite difference scheme. However, the finite difference equations based on their model must be solved by the Gauss–Seidel iterative solver. This leads to a very slow convergence rate for the numerical solution. Recently, Schneider and co-workers [3, 4] developed an 'enthalpy-like' model as well as two rules such that the enthalpy formulation can be solved by a strongly-implicit solver such as the MSI [5] and the SIS [6] solvers, while the artificial fusion temperature range is as small as 10^{-4}.

Another significant improvement on the enthalpy formulation was performed by Voller and co-workers [7–9]. In their formulation, Voller *et al.* separated the latent heat from the sensible heat. The evolution of the latent heat during a solidification process is treated as a heat source. This makes the variation of the sensible heat continuous over the entire physical domain including the liquid–solid interface. Their enthalpy formulation thus can be solved by the well-known SIMPLE algorithm [10] to obtain the sensible heat. This is a great advantage over the previous techniques. However, physically impossible results could arise in the use of Voller's method due to an improper treatment on the latent heat. This point will be discussed later.

It should be noted here that, for a PCM having a distinct freezing point, all of the existing enthalpy formulations [2–4, 7–9] predict a zigzag profile for the liquid–solid interface due to numerical error, so do the continuum model [11, 12] and the enthalpy–porosity technique [13]. This situation will be even worse when the thermal diffusivity change of the PCM is significant after solidification. Indeed, the thermal diffusivity of the solid phase is very different from that of the liquid phase for most materials. For instance, the thermal diffusivity ratios of the solid and liquid phases ($\alpha_s = \kappa_s/\kappa_l$) for common metals are 1.96 (Al), 1.77 (Cu), 0.860 (Fe), 2.08 (Zn), 1.74 (Sn). The thermal diffusivity ratio for pure water is as large as 8.77. Therefore, the thermal diffusivity jump existing at the interface cannot be neglected in solving phase change problems. The explicit enthalpy method proposed by Tacke [14] seems to produce a smoothly moving interface [15]. Unfortunately, the application of Tacke's method is restricted to one-dimensional problems with the stability criterion $\Delta\tau/\Delta x^2 \leqslant 1/3$.

In the present investigation, a new enthalpy formulation without assuming an artificial mushy zone

NOMENCLATURE

a weighting factors defined in equations (19)
B_k effective thermal resistance in $[z_{k-1}, z_k]$
C coefficient of the unsteady term in equation (17)
C_P specific heat of the PCM [J kg^{-1} K^{-1}]
E_i effective thermal resistance in $[x_i, x_{i-1}]$
F dimensionless mass flow rate
f fraction of liquid phase or dimensionless latent heat, $(H-\Lambda)/\Delta H$
$(f_P)_1$ a quarter of the fraction of the liquid phase in the region labelled '$(f_P)_1$' in Fig. 8
H, h dimensional [J kg^{-1}] and dimensionless total enthalpy, $h = H/\Delta H$
h_c dimensionless cooling coefficient at boundaries
k thermal conductivity [W m^{-1} K^{-1}]
L reference length [m]
m number of grid points in the x-coordinate
N number of continuous pieces of a piecewise continuous function in $[x_i, x_{i+1}]$
N_j effective thermal resistance in $[y_j, y_{j-1}]$
P point (x_i, y_j, z_k)
Pe Peclet number, $\rho V_c L/\kappa_1$
Q dimensionless cooling heat flux at boundaries
r location of the liquid–solid interface
r^* defined by equation (25b)
S_p, S_c coefficient of the dimensionless source term defined in equation (17)
S_j effective thermal resistance in $[y_{j-1}, y_j]$
s_n location of the nth discontinuity in $[x_i, x_{i+1}]$
Ste Stefan number, $(\Lambda_0-\Lambda_s)/\Delta H$
T temperature [K]
t time [s]
t_c characteristic time, $\rho(1+Ste^{-1})L^2/\kappa_1$
T_f freezing point of the PCM [K]
T_0, T_∞ reference temperatures with $T_s < T_f < T_0$ [K]
U, V velocities in the x- and y-direction, respectively [m s^{-1}]
u, v U/V_c, V/V_c, respectively
V_c characteristic velocity [m s^{-1}]
$w_j(Z)$ weighting function, $Z/(1-e^{-Z})$
W_i effective thermal resistance in $[x_{i-1}, x_i]$
X, Y coordinates [m]
x, y, z dimensionless coordinates
Z grid Peclet number.

Greek symbols

α dimensionless dynamic thermal diffusivity, κ/κ_1
β variable of the algebraic equation (26b)
Γ dimensionless thermal conductivity
Δ difference quantity
Δf $f-f_0$
ΔH latent heat of phase change [J kg^{-1}]
$\Delta\tau$ time step
η $(y-y_j)/\Delta y_j$
θ dimensionless temperature
θ_0 θ-value at the previous time level, $\theta(\tau-\Delta\tau)$
κ dynamic thermal diffusivity, k/C_P [kg m^{-1} s^{-1}]
Λ sensible heat defined by equation (2) [J kg^{-1}]
Λ_0 sensible heat at temperature T_0
λ dimensionless sensible heat, $(\Lambda-\Lambda_s)/(\Lambda_0-\Lambda_s)$
ξ $(x-x_i)/\Delta x_i$
ρ density of the PCM [kg m^{-3}]
σ $Ste/(1+Ste)$
τ dimensionless time, t/t_c.

Subscripts

B bottom
c characteristic quantity
E east
i, j, k quantity based on the location x_i, y_j and z_k
l liquid phase at the freezing point, T_f^+
N north
P point P
R right-hand side
S south
s solid phase at the freezing point, T_f^-
T top
x, y, z quantity, respectively, in the x-, y- and z-directions
0 quantity at the previous time $(\tau_0 = \tau-\Delta\tau)$ or at temperature T_0
∞ condition at temperature T_∞

is proposed for PCM having a distinct freezing point. As suggested by Voller [8], the latent heat is separated from the sensible heat. A rigorous method then is introduced to evaluate the latent heat inside each control volume. To account for a sharp thermal diffusivity change across the liquid–solid interface, the powerful weighting function scheme [16] is modified for solving the resulting governing equations. The performance of the present method is examined through a few examples.

ENTHALPY FORMULATION

As demonstrated by Shamsundar and Sparrow [2] and Voller and co-workers [7–9], the enthalpy equa-

tion that covers the entire physical domain including the liquid–solid interface can be written as

$$\rho\frac{\partial H}{\partial t}+\rho U\frac{\partial \Lambda}{\partial X}+\rho V\frac{\partial \Lambda}{\partial Y}=\frac{\partial}{\partial X}\left(\kappa\frac{\partial \Lambda}{\partial X}\right)+\frac{\partial}{\partial Y}\left(\kappa\frac{\partial \Lambda}{\partial Y}\right) \tag{1}$$

where H is the total enthalpy and κ the dynamic thermal diffusivity ($\kappa = k/C_P$). The sensible heat Λ defined by

$$\Lambda=\int_{T_f}^{T} C_P\,\mathrm{d}T \tag{2}$$

is a continuous function of temperature T. For convenience, the freezing point T_f has been employed for the level of sensible heat, i.e. $\Lambda_f = \Lambda(T_f) = 0$. As suggested by Voller [8], the total enthalpy is split up into latent heat and sensible heat as

$$\begin{aligned} H &= \Lambda \qquad \text{if } T < T_f \\ H &= \Lambda+\Delta H \quad \text{if } T > T_f. \end{aligned} \tag{3}$$

Note that the value of the total enthalpy H is undefined at the freezing point. After introducing the dimensionless transformation

$$\begin{gathered} x = X/L, \quad y = Y/L, \quad u = U/V_c, \quad v = V/V_c \\ \lambda = (\Lambda-\Lambda_\infty)/(\Lambda_0-\Lambda_\infty), \quad \alpha = \kappa/\kappa_l \\ Ste = (\Lambda_0-\Lambda_\infty)/\Delta H, \quad f = (H-\Lambda)/\Delta H \\ \tau = t/t_c, \quad t_c = \rho(1+Ste^{-1})L^2/\kappa_l \end{gathered} \tag{4}$$

the enthalpy equation (1) becomes

$$\begin{aligned} (1-\sigma)\frac{\partial f}{\partial \tau}+\sigma\frac{\partial \lambda}{\partial \tau}+Pe\,u\frac{\partial \lambda}{\partial x} \\ +Pe\,v\frac{\partial \lambda}{\partial y}=\frac{\partial}{\partial x}\left(\alpha\frac{\partial \lambda}{\partial x}\right)+\frac{\partial}{\partial y}\left(\alpha\frac{\partial \lambda}{\partial y}\right) \end{aligned} \tag{5}$$

where $\sigma = Ste/(1+Ste)$ and $Pe = \rho V_c L/\kappa_l$. The dimensionless latent heat f is the fraction of liquid. Its value is unity in the liquid phase and zero in the solid phase. Thus, the f-value falls from unity to zero after a liquid is completely solidified. The notations Λ_0 and Λ_∞ are, respectively, the sensible heats based on the reference temperatures T_0 and T_∞ with $T_\infty < T_f < T_0$. At the liquid–solid interface, the dimensionless sensible heat is $\lambda = \lambda_f = (1-\Lambda_0/\Lambda_\infty)^{-1}$.

It is noteworthy that in the dimensionless transformation (4), the characteristic time t_c is defined in terms of the Stefan number such that the coefficients of the two unsteady terms in equation (5) are always less than unity. Such a treatment can be expected to provide good numerical stability for any Stefan number. When the Stefan number has an infinite value ($\sigma = 1$), the latent heat term vanishes from equation (5). Therefore, the present formulation applies to single phase problems as well.

METHOD OF SOLUTION

The weighting function scheme [16] has shown good performance for heat transfer problems with variable thermal conductivity. However, it does not apply to equation (5) directly, because the dimensionless dynamic thermal diffusivity α could have a sharp discontinuity at the liquid–solid interface. To allow for such a discontinuity, the weighting function scheme is modified as follows.

Consider a one-dimensional heat transfer equation with a piecewise continuous thermal conductivity Γ in the form

$$\frac{\mathrm{d}}{\mathrm{d}x}\left(\Gamma\frac{\mathrm{d}\theta}{\mathrm{d}x}\right)-F\frac{\mathrm{d}\theta}{\mathrm{d}x}=0 \quad \text{for } x_1 \leqslant x \leqslant x_m \tag{6}$$

where the mass flow rate F is a given function of x. Let the domain be divided into $(m-1)$ intervals and let the following simple notations be used:

$$\begin{aligned} \theta_i &= \theta(x_i) \qquad \text{for } i = 1,2,\ldots,m \\ \Delta x_i &= x_{i+1}-x_i \quad \text{for } i = 1,2,\ldots,m-1 \end{aligned} \tag{7}$$

where x_i, $i = 1, 2, \ldots, m$ are the m successive points in the domain. Now, in terms of the notations, the analytical solutions for equation (6) in the intervals $[x_{i-1}, x_i]$ and $[x_i, x_{i+1}]$ are, respectively

$$\frac{\theta-\theta_{i-1}}{\theta_i-\theta_{i-1}}=\frac{\displaystyle\int_{x_{i-1}}^{x}\frac{1}{\Gamma}\exp\left(\int_{x_{i-1}}^{x}\frac{F}{\Gamma}\,\mathrm{d}x\right)\mathrm{d}x}{\displaystyle\int_{x_{i-1}}^{x_i}\frac{1}{\Gamma}\exp\left(\int_{x_{i-1}}^{x}\frac{F}{\Gamma}\,\mathrm{d}x\right)\mathrm{d}x} \tag{8}$$

$$\frac{\theta-\theta_i}{\theta_{i+1}-\theta_i}=\frac{\displaystyle\int_{x_i}^{x}\frac{1}{\Gamma}\exp\left(\int_{x_i}^{x}\frac{F}{\Gamma}\,\mathrm{d}x\right)\mathrm{d}x}{\displaystyle\int_{x_i}^{x_{i+1}}\frac{1}{\Gamma}\exp\left(\int_{x_i}^{x}\frac{F}{\Gamma}\,\mathrm{d}x\right)\mathrm{d}x}. \tag{9}$$

As discussed previously [16], the heat flux at point P (which is located at $x = x_i$) should be continuous, i.e.

$$\Gamma_i^+(\partial\theta/\partial x)_i^+ = \Gamma_i^-(\partial\theta/\partial x)_i^- \tag{10}$$

where Γ_i^+ and Γ_i^- are the Γ values at the locations x_i^+ and x_i^-, respectively. Substitution of equations (8) and (9) into equation (10) yields the numerical scheme for point P

$$\left[\frac{\mathrm{d}}{\mathrm{d}x}\left(\Gamma\frac{\mathrm{d}\theta}{\mathrm{d}x}\right)-F\frac{\mathrm{d}\theta}{\mathrm{d}x}\right]_i=(a_W)_i\theta_{i-1}+(a_P)_i\theta_i+(a_E)_i\theta_{i+1}$$

$$\begin{aligned} (a_W)_i &= (W_i\overline{\Delta x}_i)^{-1} \\ (a_E)_i &= (E_i\overline{\Delta x}_i)^{-1} \\ (a_P)_i &= -(a_W)_i-(a_E)_i \end{aligned} \tag{11}$$

where the subscript i denotes quantities relating to point P and $\overline{\Delta x}_i = (\Delta x_{i-1}+\Delta x_i)/2$ is the size of the 'control volume' containing point P. The notation

$(a_W)_i$ is the weighting factor of the point $x = x_{i-1}$ (the nearest grid point lying to the *west* of point P) when the differential equation (6) is discretized at point P. The notation $(a_E)_i$ is defined similarly with the subscript E denoting *east*. The symbols W_i and E_i, respectively, represent the integrations

$$W_i = \int_{x_{i-1}}^{x_i} \frac{1}{\Gamma} \exp\left(-\int_x^{x_i} \frac{F}{\Gamma}\,dx\right) dx \qquad (12a)$$

$$E_i = \int_{x_i}^{x_{i+1}} \frac{1}{\Gamma} \exp\left(\int_{x_i}^{x} \frac{F}{\Gamma}\,dx\right) dx. \qquad (12b)$$

Equation (11) demonstrates that the sum of conduction and convection terms in the x-direction can be discretized into an algebraic relationship among the temperatures of point P and its two neighbouring points W and E. A similar situation exists in the y- and z-directions.

It is interesting to note from equations (12) that, when the mass flow rate is zero ($F = 0$), W_i becomes the total thermal resistance in the interval $[x_{i-1}, x_i]$ that lies to the *west* of point P. For convenience, this particular interval will be referred to as 'the west-side interval of point P'. Likewise, E_i is the total thermal resistance in $[x_i, x_{i+1}]$, the east-side interval of point P. An increase in the thermal conductivity Γ in the west-side interval can be seen to decrease the total thermal resistance W_i for that interval. This leads to an increase in the weighting factor $(a_W)_i$ (see equation (11)) such that θ_{i-1} has a larger influence on the value of θ_i. A similar phenomenon exists for the thermal resistance E_i in the east-side interval. In the presence of a mass flow, say from west to east ($F > 0$), W_i becomes the effective thermal resistance that is smaller than the true thermal resistance as can be verified from equation (12a). In contrast, this mass flow gives an effective thermal resistance E_i that is larger than the true one for the east-side interval, see equation (12b). For the limiting case of $F = \infty$, one obtains $W_i = 0$ and $E_i = \infty$ such that equations (11) become the fully upwind scheme. This behaviour is consistent with physical reasoning.

It is noted that the application of scheme (11) and (12) is restricted to internal points ($i = 2, 3, \ldots, m-1$) due to the use of equation (10). For a Dirichlet boundary condition, no additional treatment is needed at the boundary. However, this is not justified for Neumann and Cauchy boundary conditions. Let h_c be a *cooling* coefficient and Q be a *cooling* heat flux imposed on the boundaries, i.e.

$$\Gamma_1^+ (\partial\theta/\partial x)_1^+ = h_c\theta_1 + Q \quad \text{at } x = x_1 \qquad (13a)$$

$$-\Gamma_m^- (\partial\theta/\partial x)_m^- = h_c\theta_m + Q \quad \text{at } x = x_m. \qquad (13b)$$

It is not surprising that with the aid of equations (8) and (9), both equations (13a) and (13b) provide the same algebraic form for $i = 1$ and m

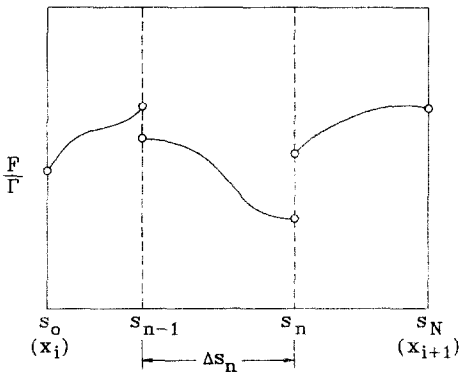

FIG. 1. A schematic F/Γ function with discontinuities in the interval $[x_i, x_{i+1}]$.

$$\left[\frac{d}{dx}\left(\Gamma\frac{d\theta}{dx}\right) - F\frac{d\theta}{dx}\right]_i = (a_W)_i\theta_{i-1} + (a_P)_i\theta_i + (a_E)_i\theta_{i+1} - (a_R)_i$$

$$(a_W)_i = (W_i\Delta x_i)^{-1}$$

$$(a_E)_i = (E_i\Delta x_i)^{-1}$$

$$(a_P)_i = -(a_W)_i - (a_E)_i - h_c/\Delta x_i$$

$$(a_R)_i = Q/\Delta x_i \qquad (14)$$

where $(a_W)_1 = (a_E)_m = 0$, $\Delta x_1 = \Delta x_1/2$ and $\Delta x_m = \Delta x_{m-1}/2$.

It appears that the numerical scheme (equations (11), (12) and (14)) could produce an exact solution for equation (6). This is true even for composite materials with thermal contact resistance between two adjacent layers. However, under many practical situations, the integrations in equations (12) cannot be performed analytically. Fortunately, a simple approximation can be drawn from the exact scheme. Suppose the piecewise continuous function F/Γ has N continuous sub-intervals separated by $N-1$ discontinuities located at $x = s_n$, $n = 1, 2, \ldots, N-1$ in the interval $[x_i, x_{i+1}]$ as shown in Fig. 1. Performing the integration in equation (12b) piece by piece, one arrives at

$$E_i = \sum_{n=1}^{N} \int_{s_{n-1}}^{s_n} \frac{1}{\Gamma} \exp\left(\int_{s_0}^{x} \frac{F}{\Gamma}\,dx\right) dx$$

$$= \sum_{n=1}^{N} \frac{\Delta s_n}{\Gamma(s_{n-1}^+)} \frac{1}{w_f(Z_n)} \exp\left(\int_{s_0}^{s_{n-1}} \frac{F}{\Gamma}\,dx\right) \qquad (15a)$$

$$Z_n = \int_{s_{n-1}}^{s_n} \left(\frac{1}{\Gamma}\frac{d\Gamma}{dx} - \frac{F}{\Gamma}\right) dx \approx (\Delta s_n)\left(\frac{1}{\Gamma}\frac{d\Gamma}{dx} - \frac{F}{\Gamma}\right) \qquad (15b)$$

where $s_0 = x_i$, $s_N = x_{i+1}$ and $\Delta s_n = s_n - s_{n-1}$. The parameter Z_n defined by equation (15b) is the grid Peclet number in the sub-interval $[s_{n-1}, s_n]$ with the 'bar' denoting the mean value of a quantity in that sub-interval. The function $w_f(Z) = Z/(1-\exp(-Z))$

known as the weighting function [16] can be efficiently computed from the power law [10]

```
FUNCTION WF(Z)
WF = 0.
IF (Z.GT.0.) WF = Z
A = ABS(Z)
IF (A.LT.10.) WF = WF+(1.-0.1*A)**5
RETURN
END
```
(15c)

The accuracy of the power-law approximation (15c) has been well discussed in ref. [16]. By a similar procedure, the expression of W_{i+1} for the same interval becomes

$$W_{i+1} = \sum_{n=1}^{N} \frac{\Delta s_n}{\Gamma(\bar{s_n})} \frac{1}{w_f(-Z_n)} \exp\left(-\int_{s_n}^{s_N} \frac{F}{\Gamma} \mathrm{d}x\right). \tag{16}$$

In fact, the integrations remaining in equations (15a) and (16) are difficult to compute in many practical problems, because both F and Γ have known values only at discrete points. Fortunately, the exponential functions can be removed under some particular situations. For instance, for the case of no discontinuity ($N = 1$), the summation has only one term. The exponential functions thus do not appear in equations (15a) and (16) such that the present formulation reduces to the weighting function scheme proposed previously [16]. For the case of pure heat conduction ($F = 0$), the integration becomes zero and thus the value of the exponential function is unity. In practical problems dealing with conjugate heat transfer or phase change, a thermal conductivity jump and/or a thermal contact resistance exists only at the fluid–solid interface. Fortunately, the mass flow normal to the fluid–solid interface is very small in general if there is no suction or blowing at the solid boundary. Therefore, the values of the exponential functions are essentially equal to unity for a grid interval containing a fluid–solid interface. In fact, even if the exponential functions are removed, the effect of the fluid flow is still taken into account through the use of the weighting function $w_f(Z)$. For particular situations when the exponential functions in equations (15a) and (16) are not negligible, the integrations can be performed simply by using the trapezoidal rule.

For an unsteady three-dimensional conservation equation having a piecewise continuous thermal conductivity Γ in the form

$$C\frac{\partial\theta}{\partial t} + F_x\frac{\partial\theta}{\partial x} + F_y\frac{\partial\theta}{\partial y} + F_z\frac{\partial\theta}{\partial z} = \frac{\partial}{\partial x}\left(\Gamma\frac{\partial\theta}{\partial x}\right) + \frac{\partial}{\partial y}\left(\Gamma\frac{\partial\theta}{\partial y}\right) + \frac{\partial}{\partial z}\left(\Gamma\frac{\partial\theta}{\partial z}\right) - (S_p\theta + S_c) \tag{17}$$

the discretization equation based on the weighting function scheme (11) and (14)–(16) for point P(x_i, y_j, z_k) is

$$a_W\theta_{i-1,j,k} + a_E\theta_{i+1,j,k} + a_S\theta_{i,j-1,k} + a_N\theta_{i,j+1,k} + a_B\theta_{i,j,k-1} + a_T\theta_{i,j,k+1} + a_P\theta_{i,j,k} = a_R \tag{18}$$

$$a_W = (W_i\overline{\Delta x_i})^{-1}, \quad a_E = (E_i\overline{\Delta x_i})^{-1}$$

$$a_S = (S_j\overline{\Delta y_j})^{-1}, \quad a_N = (N_j\overline{\Delta y_j})^{-1}$$

$$a_B = (B_k\overline{\Delta z_k})^{-1}, \quad a_T = (T_k\overline{\Delta z_k})^{-1}$$

$$a_P = -a_W - a_E - a_S - a_N - a_B - a_T - (S_p + C/\Delta t)_{i,j,k}$$

$$a_R = (S_c - C\theta_0/\Delta t)_{i,j,k} \tag{19}$$

where the subscript '0' stands for a quantity at the previous time ($t_0 = t - \Delta t$) and i, j, k for a quantity at point P. As in the one-dimensional case, the coefficient a_W is the weighting factor of the nearest grid point located to the *west* of point P. Similarly, subscripts E, S, N, B, T, P and R appearing in a_E, a_S, a_N, a_B, a_T, a_P and a_R denote, respectively, east, south, north, bottom, top, point P and the quantity at the right-hand side of equation (18). It should be noted that in equations (18) and (19) the subscript i, j, k has been deleted from the notation of the weighting factors for simplicity, i.e. a_W denotes $(a_W)_{i,j,k}$, etc. Such a symbolic system has been well accepted [10].

In equations (19), the effective thermal resistances in the east-side interval $[x_i, x_{i+1}]$ of point P(x_i, x_j, z_k) are expressible as

$$W_{i+1} = \sum_{n=1}^{N} \frac{\Delta s_n}{\Gamma(s_n^-)} \frac{1}{w_f(-Z_n)} \tag{20a}$$

$$E_i = \sum_{n=1}^{N} \frac{\Delta s_n}{\Gamma(s_{n-1}^+)} \frac{1}{w_f(Z_n)}. \tag{20b}$$

As mentioned earlier, when both Γ and F have no discontinuity inside the interval $[x_i, x_{i+1}]$, the present formulation will reduce to the standard weighting function scheme [16], i.e.

$$(a_W)_{i+1,j,k} = [\Gamma(x_{i+1}^-)/(\Delta x_i\overline{\Delta x_{i+1}})]w_f(-Z_{i+1/2}) \tag{21a}$$

$$(a_E)_{i,j,k} = [\Gamma(x_i^+)/(\Delta x_i\overline{\Delta x_i})]w_f(Z_{i+1/2}) \tag{21b}$$

where $Z_{i+1/2}$ is the grid Peclet number in the interval $[x_i, x_{i+1}]$. The expressions for the effective thermal resistances in the south-, north-, bottom- and top-side intervals (i.e. S_j, N_j, B_k and T_k) are similar to equations (20) and (21). However, they are not shown here to conserve space. For better efficiency in the computations, the weighting factors $(a_W)_{i+1,j,k}$ and $(a_E)_{i,j,k}$ (or the effective thermal resistances $W_{i+1,j,k}$ and $E_{i,j,k}$) in the interval $[x_i, x_{i+1}]$ can be computed simultaneously by using the important property of the weighting function, $w_f(Z) = Z + w_f(-Z)$.

PERFORMANCE OF THE NEW METHOD

In practical phase change problems, both thermal conductivity and specific heat are functions of temperature. Their values could have a sharp discontinuity across the liquid–solid interface in a PCM having a distinct freezing point. Under such a situation, the present enthalpy formulation (5) along with the modified weighting function scheme (18)–(21) can be expected to have good performance. In this section, a one-dimensional phase change problem is illustrated in Example 1 to examine the performance of the present numerical technique. The result will be compared with that based on the existing methods. Example 2 is conducted to study the performance of the present method in a two-dimensional case without natural convection in the liquid phase. The numerical technique for three-dimensional solidification is similar to that for a two-dimensional case. Hence, no three-dimensional example is given here. In the presence of natural convection, the mass, momentum and energy equations are strongly coupled. The major difficulty in solving such a problem is to satisfy the no-slip boundary condition at the liquid–solid interface that has an irregular profile. In addition, the velocity gradient has a discontinuity across the interface. Such difficulties require a particular numerical technique. For convenience, a solidification problem dealing with natural convection will be studied in ref. [17].

Example 1. *Solidification in a half-space*

It is customary to test a numerical method by choosing a simple model problem that possesses an analytical solution. For this purpose, consider a liquid in the half-space ($X \geqslant 0$) at a uniform temperature above the freezing point. At time $t \geqslant 0$, a temperature below the freezing point of the liquid is imposed on the boundary surface at $X = 0$. Solidification thus starts from $X = 0$ with a liquid–solid interface moving in the positive X-direction. The thermal properties could have significant changes after the liquid has solidified. However, both liquid and solid phases are assumed to have their own constant thermal properties such that an analytic solution exists for the problem.

After applying the dimensionless transformation (4), the governing equation and the associated boundary conditions can be written as

$$(1-\sigma)\frac{\partial f}{\partial \tau}+\sigma\frac{\partial \lambda}{\partial \tau}=\frac{\partial}{\partial x}\left(\alpha\frac{\partial \lambda}{\partial x}\right)$$

$$\lambda(x,0)=1,\quad \lambda(0,\tau)=0,\quad \lambda(\infty,\tau)=1$$

$$f(x,0)=1 \tag{22}$$

where the notations are the same as defined in the previous section. Applying the weighting function scheme (11) on the x-derivatives of equation (22) and the backward difference on the unsteady terms, one obtains the algebraic equations for the point x_i

$$a_W\lambda_{i-1}+a_P\lambda_i+a_E\lambda_{i+1}=a_R$$

$$a_W=(W_i\Delta x_i)^{-1},\quad a_E=(E_i\Delta x_i)^{-1}$$

$$a_P=-a_W-a_E-\sigma/\Delta\tau$$

$$a_R=[(1-\sigma)/\Delta\tau][f_i-(f_0)_i]-(\sigma/\Delta\tau)(\lambda_0)_i \tag{23}$$

where the subscript '0' denotes a quantity at the previous time ($\tau_0=\tau-\Delta\tau$) and the effective thermal resistance W_i and E_i are defined by equations (20).

It is noted that the values of W_i, E_i and f_i appearing, respectively, in the expressions of a_W, a_E and a_R are not known. An iterative procedure thus is needed in solving equations (23). For a guessed $\lambda(x)$ solution, the location of the liquid–solid interface can be estimated by using the energy conservation law at the interface

$$\alpha_s\left(\frac{\partial \lambda}{\partial x}\right)_s-\left(\frac{\partial \lambda}{\partial x}\right)_l=(1-\sigma)\frac{\mathrm{d}r}{\mathrm{d}\tau} \tag{24}$$

where $r(\tau)$ is the location of the liquid–solid interface and the subscripts s and l stand for, respectively, quantities at $x=r^-$ and r^+. Suppose phase change is taking place inside the interval $[x_i, x_{i+1}]$, i.e. $\lambda_i<\lambda_f<\lambda_{i+1}$ and $x_i<r<x_{i+1}$. Assuming linear λ variation in each of the liquid and solid phases, that is $(\partial\lambda/\partial x)_s=(\lambda_f-\lambda_i)/(r-x_i)$ and $(\partial\lambda/\partial x)_l=(\lambda_{i+1}-\lambda_f)/(x_{i+1}-r)$, one obtains

$$r=r^*-\frac{(1-\sigma)(r-x_i)(x_{i+1}-r)}{\alpha_s(\lambda_f-\lambda_i)+(\lambda_{i+1}-\lambda_f)}\frac{r-r_0}{\Delta\tau} \tag{25a}$$

$$r^*=x_i+\frac{\alpha_s(\lambda_f-\lambda_i)\Delta x_i}{\alpha_s(\lambda_f-\lambda_i)+(\lambda_{i+1}-\lambda_f)}. \tag{25b}$$

The cubic polynomial (25a) seems to be rigorous for estimating the r-value. Unfortunately, equations (25) do not guarantee a root of r exists in the interval $[x_i, x_{i+1}]$ especially when the guessed $\lambda(x)$ is not sufficiently accurate. This could eventually lead to a diverging result for the $\lambda(x)$ solution. In the present formulation, the contribution due to the unsteady term on the right-hand side of equation (24) is neglected. Equation (25a) thus reduces to

$$r=r^* \tag{25c}$$

such that a unique r-value exists in the interval $[x_i, x_{i+1}]$. This simplified interpolation procedure would result in a numerical error when the solidification speed $\mathrm{d}r/\mathrm{d}\tau$ is large and/or the Stefan number is small ($\sigma \approx 0$). Figure 2 shows a typical $\lambda(x)$ distribution based on the characteristics of the exact solution [18]. Fortunately, as can be observed from Fig. 2, this interpolation error ($r-r^*=\Delta r$) would always be less than the grid size Δx_i.

It should be noted here that the effect of the moving liquid–solid interface on the sensible heat λ has been taken into account through the unsteady term $(1-\sigma)\partial f/\partial\tau$ on the left-hand side of equation (22). The use of equation (24) is only for interpolating the liquid–solid interface from the updated λ-result.

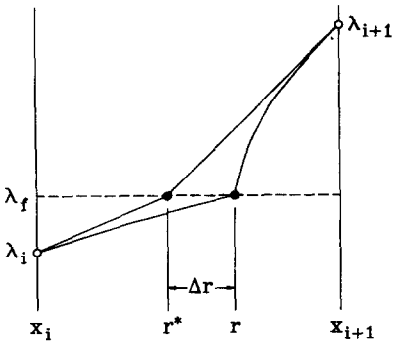

FIG. 2. Numerical error in locating the liquid–solid interface due to linear interpolation (25b) and (25c).

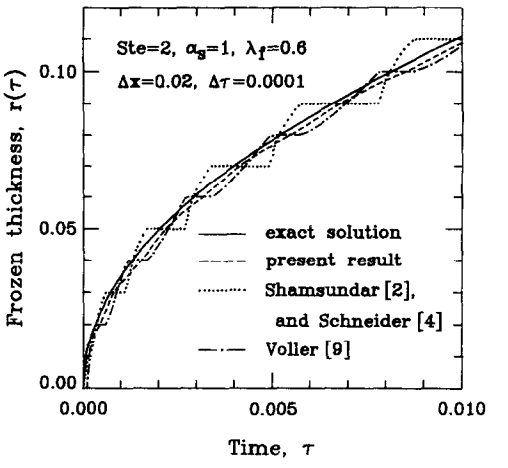

FIG. 4. Comparisons of the frozen thickness among various methods for the case of $Ste = 2$, $\alpha_s = 1$ and $\lambda_f = 0.6$.

Hence, equation (25c) can be expected to be a good approximation as long as the grid size Δx_i is sufficiently small. Once the interface location (the r-value) is determined, the effective thermal resistances W_i and E_i are updated from equations (20). Thanks to the use of the thermal resistances W_i and E_i, the present scheme always provides a good numerical stability in spite of the discontinuity in the α-value at the liquid–solid interface.

A sharp discontinuity exists also in the f-value. As mentioned earlier, the f-value at a point will fall from unity to zero when the liquid–solid interface sweeps through that point. Unfortunately, the abrupt change in the f-value could cause a serious numerical instability. A control volume thus is required in estimating the f-value for a grid point. Let the dashed lines shown in Fig. 3 be the boundaries of the control volumes for a one-dimensional problem. The ith control volume having the size $\overline{\Delta x}_i$ contains the point x_i. At a time τ, the liquid–solid interface (denoted by the vertical solid line) is assumed to be in the ith control volume. To achieve a smoothly varying f-value in the computations, the fraction of the liquid phase inside the ith control volume is employed as the value of f_i instead of the true value $f(x_i)$. The difference $(f_0)_i - f_i$ thus is the fraction of the ith control volume solidified during the time interval $[\tau_0, \tau]$. In the present example, owing to the Dirichlet condition imposed at the boundary $x = x_1$, no governing equation is needed at the point x_1. This leads to a failure in handling the latent heat released from the region $x_1 \leqslant x \leqslant (x_1 + x_2)/2$. To properly treat the latent heat, the size of the control volume containing the point x_2 is defined by $\overline{\Delta x}_2 = (x_2 + x_3)/2 - x_1$ (see the hatched region in Fig. 3). When a uniform grid system ($\overline{\Delta x}_i = \Delta x_i = \Delta x$) is employed, the value of $\overline{\Delta x}_2$ reduces to $\overline{\Delta x}_2 = (3/2)\Delta x$. This particular treatment, however, is not necessary if the grid size along the boundaries is sufficiently small.

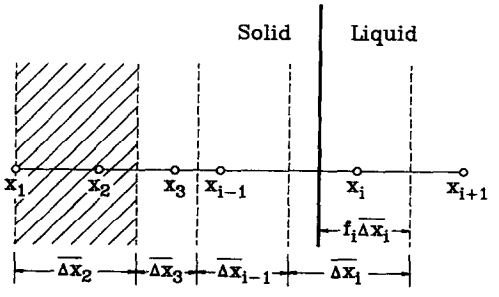

FIG. 3. Definitions for the control volumes and for the f-value of the ith control volume where phase change is taking place.

For convenience, the present numerical algorithm is summarized as follows. Guess a $\lambda(x)$ solution for an instant time τ. The corresponding liquid–solid interface is then located by assuming $r = r^*$. Based on this interface location, the f-value is evaluated from the fraction of liquid inside each control volume. Next, compute the weighting factors from equations (19) and (20) and then renew the $\lambda(x)$ result by solving equations (23). This procedure should be repeated until the $\lambda(x)$ results converge within a prescribed tolerance. In the present study, the computation is terminated when four-place accuracy is achieved for the $\lambda(x)$ results. Generally speaking, an SOR (successive over-relaxation) factor in the range of 0.1–0.3 is needed for the $\lambda(x)$ result during the iterations.

Figure 4 reveals the present $r(\tau)$ result and that evaluated from the analytical solution [18]

$$r(\tau) = 2\beta(\tau/\sigma)^{1/2} \tag{26a}$$

$$\frac{\lambda_f \exp(-\beta^2)}{\operatorname{erf}(\beta)} - \frac{(1-\lambda_f)\alpha_s^{-1/2}\exp(-\beta\alpha_s)}{\operatorname{erfc}(\beta\alpha_s^{1/2})} - \frac{\pi^{1/2}\beta}{Ste} = 0 \tag{26b}$$

for the case of $Ste = 2$, $\alpha_s = 1$ and $\lambda_f = 0.6$. The numerical results based on the existing enthalpy formulations by Shamsundar and Sparrow [2], Schneider [4] and Voller *et al.* [9] are also plotted in Fig. 4 for comparisons. The discrepancy between the results based on the algorithms by Shamsundar and Sparrow

[2] and by Schneider [4] is less than 0.1%. Thus, a single curve is used to represent both results. Note that both the present formulation and the analytical solution (26) do not depend on the individual values of k_s/k_l and $(C_p)_s/(C_p)_l$. These particular values, however, are required in the use of the conventional enthalpy formulations [2, 4]. The parameters $k_s/k_l = (C_p)_s/(C_p)_l = 1$ thus were employed instead of $\alpha_s = 1$ in the solution procedures of refs. [2, 4]. In all of the computations, the step sizes $\Delta x = 0.02$ and $\Delta\tau = 0.0001$ were used.

From Fig. 4, all of the existing enthalpy formulations [2, 4, 9] are seen to provide zigzag variations for the frozen thickness $r(\tau)$. In the conventional enthalpy formulations [2, 4, 9], the enthalpy change at a grid point is regarded as the latent heat released from the corresponding control volume of that grid point. As a result, a control volume will 'suddenly' release its entire latent heat at the instant while the liquid–solid interface is sweeping through its grid point. This will result in a zigzag function for $r(\tau)$ with jumps having the size of $\Delta x = 0.02$. Such jumps can be clearly observed from Fig. 4. Although these unphysical zigzags in the interface-time results can be smoothed by applying a curve-fitting technique after the solution converges (see Shamsundar and Rooz [19], for example), they usually cause a very slow convergence rate during the iterations. In the present technique, the dimensionless latent heat (the f-value) for each control volume is rigorously evaluated such that the latent heat can be released 'evenly'. This might account for the fact that the present numerical technique produces a smooth function for the frozen thickness (see Fig. 4) with a fast convergence rate. From Fig. 4, one sees also that the present numerical technique slightly underpredicts the frozen thickness $r(\tau)$. This error is believed to arise from the simplified interpolation procedure (25c) at the very beginning of the solidification process, i.e. $\tau < 0.001$. In the region $\tau > 0.001$, the solidification rate is not large such that equation (25c) becomes a good approximation in locating the liquid–solid interface. Therefore, the curve of the present result is essentially parallel to that of the exact solution in the region of $\tau > 0.001$. Fortunately, this error can be eliminated by reducing the step sizes Δx and $\Delta\tau$ as long as the parameter $(1-\sigma)(\Delta x)^2/\Delta\tau$ is maintained at a value of less than 0.2. The reasoning will be discussed later.

As mentioned in the previous paragraph, the jumps in the zigzag $r(\tau)$ profiles based on refs. [2, 4, 9] are equal to the spatial step size Δx employed in the computations. Hence, the conventional formulations are expected to provide good numerical results as long as the grid size Δx is sufficiently small. However, this seems not to be true in the use of the algorithm by Voller *et al.* [9] when a large thermal diffusivity jump exists at the liquid–solid interface ($\alpha_s \gg 1$). To clarify this point, the $r(\tau)$ results for the case of $Ste = 0.5$, $\alpha_s = 10$ and $\lambda_f = 0.8$ are presented in Fig. 5. In the use of the algorithms by Shamsundar and Sparrow [2] and Schneider [4], the parameters $k_s/k_l = 5$ and $(C_p)_s/(C_p)_l = 0.5$ are employed instead of $\alpha_s = 10$. The grid system used for all of the computations is $\Delta x = 0.01$ and $\Delta\tau = 0.0005$. From Fig. 5, a good agreement between the present result and that evaluated from the analytical solution (26) is once again observed. The jumps in the $r(\tau)$ profiles produced by the algorithms of refs. [2, 4, 9] are seen to reduce to $\Delta x = 0.01$. However, the algorithm by Voller *et al.* [9] underpredicts the $r(\tau)$ values by a great amount which cannot be improved by reducing the spatial step size Δx.

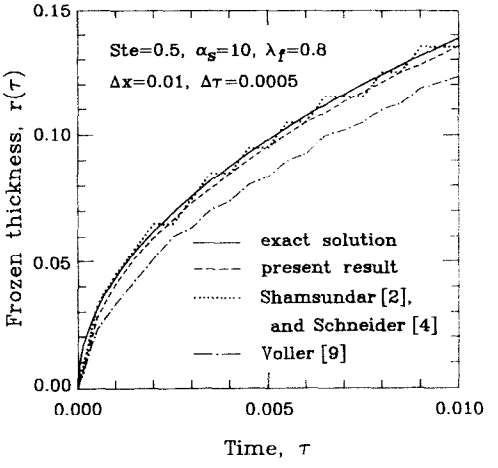

FIG. 5. Comparisons of the frozen thickness among various methods for the case of $Ste = 0.5$, $\alpha_s = 10$ and $\lambda_f = 0.8$.

In their enthalpy formulation, Voller *et al.* [9] split up the enthalpy H into sensible heat Λ and latent heat ΔH with the enthalpy level $H_f = \Lambda_f = 0$. For simplicity, the latent heat at a grid point was regarded as the average latent heat of the control volume containing that grid point. Hence, a grid point could have a dimensionless latent heat in the range of $0 \leqslant f \leqslant 1$. Under such a treatment, the latent heat of each grid point must be guessed before the energy equation can be solved to yield the sensible heat as demonstrated previously. This sensible heat then was added to the guessed latent heat to form the total enthalpy $h(x)$. Finally, Voller *et al.* [8, 9] renewed the latent heat distribution from the updated total enthalpy by making the assumption

$$\begin{aligned} f &= 0 \quad \text{if } h \leqslant 0 \\ f &= h \quad \text{if } 0 \leqslant h \leqslant 1 \\ f &= 1 \quad \text{if } h \geqslant 1 \end{aligned} \tag{27}$$

where $h = H/\Delta H$. This procedure was iterated until the solution converged within a prescribed tolerance. Obviously, Voller's assumption (27) allows a phase change to take place inside more than one control volume at the same time especially when the value of the Stefan number is small. This could happen even for $\alpha_s = 1$. As an example, the case of $Ste = 0.5$, $\alpha_s = 1$ and $\lambda_f = 0.5$ is solved by using Voller's algorithm with

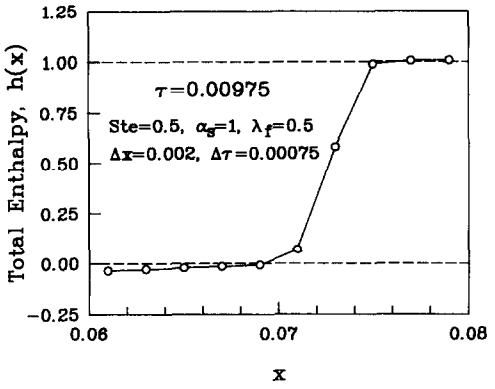

FIG. 6. The result of total enthalpy at $\tau = 0.00975$ based on Voller's algorithm [9] and the parameters $Ste = 0.5$, $\alpha_s = 1$ and $\lambda_f = 0.5$.

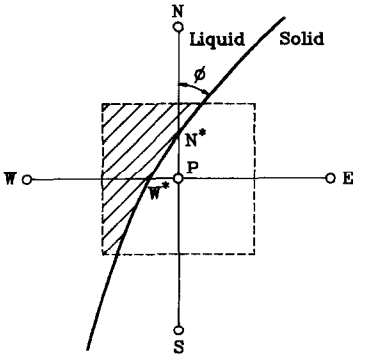

FIG. 7. Definition of the f-value for a two-dimensional control volume.

the step size $\Delta x = 0.002$ and $\Delta\tau = 0.00075$. Figure 6 shows the result of the dimensionless total enthalpy $h(x)$ for the time instance $\tau = 0.00975$. From Fig. 6, it can be seen that the phase change is taking place inside three control volumes at the same time. This is physically impossible for a PCM having a distinct freezing point. Such a situation is even worse when $\alpha_s \neq 1$. Thus, the great numerical error produced by Voller's algorithm [9] in Fig. 5 is believed to arise from the improper assumption (27).

Example 2. *Solidification in a two-dimensional corner*

Consider a quarter-space ($X \geqslant 0$ and $Y \geqslant 0$) of liquid initially at a uniform temperature T_0. For time $t \geqslant 0$, the surfaces $X = 0$ and $Y = 0$ are maintained at a constant temperature T_∞ that is below the freezing point of the liquid. Solidification thus occurs from the corner of the quarter-space at $t \geqslant 0$. After introducing the dimensionless transformation (4), the physical problem becomes

$$(1-\sigma)\frac{\partial f}{\partial \tau} + \sigma\frac{\partial \lambda}{\partial \tau} = \frac{\partial}{\partial x}\left(\alpha\frac{\partial \lambda}{\partial x}\right) + \frac{\partial}{\partial y}\left(\alpha\frac{\partial \lambda}{\partial y}\right)$$

$$\lambda(0, y, \tau) = \lambda(x, 0, \tau) = 0$$

$$\lambda(\infty, y, \tau) = \lambda(x, \infty, \tau) = 1$$

$$\lambda(x, y, 0) = 1, \quad f(x, y, 0) = 1. \qquad (28)$$

It appears that the system of equations (28) can be solved by using the weighting function scheme (18) and (19). For simplicity, a uniform grid system ($\Delta x = \Delta y$) is employed here. After this is done, the resulting algebraic equations are

$$a_W\lambda_{i-1,j} + a_E\lambda_{i+1,j} + a_S\lambda_{i,j-1} + a_N\lambda_{i,j+1} + a_P\lambda_{i,j} = a_R$$

$$a_W = \Delta x/W_i, \quad a_E = \Delta x/E_i$$

$$a_S = \Delta x/S_j, \quad a_N = \Delta x/N_j$$

$$a_P = -a_W - a_E - a_S - a_N - \sigma(\Delta x)^2/\Delta\tau$$

$$a_R = [(\Delta x)^2/\Delta\tau][(1-\sigma)(\Delta f)_{i,j} - \sigma(\lambda_0)_{i,j}] \qquad (29)$$

where $(\Delta f)_{i,j} = f_{i,j} - (f_0)_{i,j}$. As in Example 1, the dimensionless thermal diffusivity α is assumed to have a value of unity in the liquid phase and a constant value denoted by α_s in the solid phase. Equations (29) always produce a matrix equation with a diagonally dominated coefficient matrix. However, before applying the numerical scheme, care must be exercised in evaluating the f-value for a given $\lambda(x, y)$ distribution.

The latent heat term $(1-\sigma)\partial f/\partial\tau$ appearing in equation (28), in fact, is a moving line source. Suppose the liquid–solid interface moves from curve A to curve B during a time step $\Delta\tau$. This means that the liquid inside the region bounded by curves A and B gives away its latent heat and solidifies after the time step $\Delta\tau$. In the present formulation, the function $f(x, y)$ is employed to handle the latent heat released in each time step. The value of $f(x, y)$ is unity in the liquid region and zero in the solid region. This implies that the difference $f_0(x, y) - f(x, y) = -\Delta f$ has a value of unity inside the region bounded by curves A and B, while it is zero outside that particular region. Therefore, the line source can be well modelled by the distribution $-\Delta f$ with the intensity $(1-\sigma)/\Delta\tau$. However, when a numerical method is applied on equation (28), the f-value might jump between zero and unity at a grid point if the interface is passing through that point during the iterations. This could cause a very slow convergence rate or even a divergent solution as encountered in most previous works. Fortunately, this numerical difficulty can be remedied by assuming the $f_{i,j}$ value at a grid point (x_i, y_j) to be the fraction of the liquid phase inside the control volume of that point instead of its true value $f(x_i, y_j)$, as has been done in Example 1 for the one-dimensional case.

Suppose that at an instant a phase change front intersects the segments of lines $\overline{PN}$ and $\overline{PW}$ at points N* and W*, respectively, as illustrated in Fig. 7. As demonstrated in ref. [18], the energy balance at point N* can be written as

$$\alpha_s\left(\frac{\partial \lambda}{\partial y}\right)_s - \left(\frac{\partial \lambda}{\partial y}\right)_l = \sin^2\phi(1-\sigma)\frac{dr}{d\tau} \qquad (30)$$

where r is the y-coordinate of point N* and ϕ the intersection angle between the phase change front and

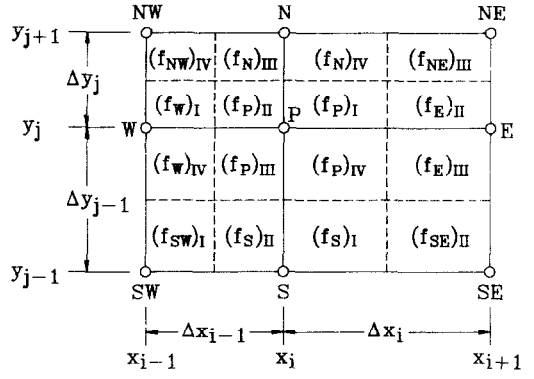

FIG. 8. Definition for the four quadrants of a control volume; $(f_P)_I$ is a quarter of the fraction of the liquid phase in the region labelled '$(f_P)_I$'.

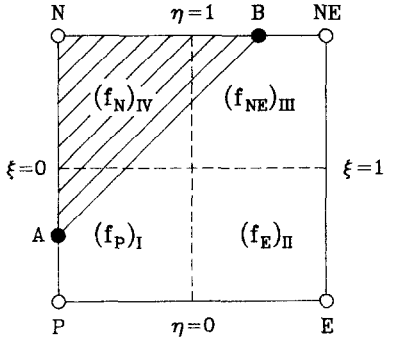

FIG. 9. The transformed unit grid cell P–E–NE–N–P in (ξ, η) coordinates.

segment of line $\overline{PN}$ (see Fig. 7). It is interesting to note that equation (30) will reduce to equation (25c), if the unsteady term on the right-hand side of equation (30) is neglected and the λ variation is assumed linear in each of the liquid and solid phases. Therefore, the phase change front (point N*) can be located as in a one-dimensional case. With a similar manner, the location of point W* is determined.

After the location of the liquid–solid interface is known, the f-value for point P (i.e. f_P) defined by the fraction of the liquid phase inside the control volume P (see the hatched region shown in Fig. 7) can be simply evaluated by dividing the control volume P into four quadrants. In terms of the notations defined in Fig. 8, the value of f_P is expressible as

$$f_P = [(f_P)_I \Delta x_i \Delta y_j + (f_P)_{II} \Delta x_{i-1} \Delta y_j + (f_P)_{III} \Delta x_{i-1} \Delta y_{j-1} + (f_P)_{IV} \Delta x_i \Delta y_{j-1}]/(\Delta x_i \Delta y_j) \quad (31)$$

where $(f_P)_I \Delta x_i \Delta y_j$ is the area of the liquid phase in the region labelled '$(f_P)_I$' in Fig. 8. For numerical convenience, the grid cell P–E–NE–N–P is mapped onto a unit square in (ξ, η) coordinates as shown in Fig. 9 by employing the linear transformation $\xi = (x - x_i)/\Delta x_i$ and $\eta = (y - y_j)/\Delta y_j$. Hence, $(f_P)_I$ is the area of the liquid phase (the hatched region in Fig. 9) in the region $0 \leqslant \xi \leqslant 0.5$ and $0 \leqslant \eta \leqslant 0.5$. The values of $(f_E)_{II}$, $(f_{NE})_{III}$ and $(f_N)_{IV}$ have similar physical meanings.

Next, consider the condition that phase change is taking place inside the grid cell P–E–NE–N–P. It should be noted here that the liquid–solid interface will intersect the boundary of the grid cell at just two points as long as this cell is sufficiently small. Suppose $\lambda_N > \lambda_f > \lambda_P$ and $\lambda_N > \lambda_f > \lambda_{NE}$ such that the interface intersects the grid cell boundary at points A and B as illustrated in Fig. 9. For simplicity, the straight line $\overline{AB}$ is adopted to approximate the interface profile. From Fig. 9, it can be seen that the values of $(f_P)_I$, $(f_E)_{II}$, $(f_{NE})_{III}$ and $(f_N)_{IV}$ depend only on the locations of points A and B. For instance, $(f_P)_I = 1/32$, $(f_E)_{II} = 0$, $(f_{NE})_{III} = 1/32$ and $(f_N)_{IV} = 7/32$ if the locations of A and B in (ξ, η) coordinates are $(0, 1/4)$ and $(3/4, 1)$. In case all of the λ-values at the four corners are larger than λ_f, then assign $(f_P)_I = (f_E)_{II} = (f_{NE})_{III} = (f_N)_{IV} = 0.25$. Similarly, assign $(f_P)_I = (f_E)_{II} = (f_{NE})_{III} = (f_N)_{IV} = 0$ if all of the λ-values at the corners are smaller than λ_f.

After applying this procedure on all of the grid cells, the f-values at each grid point can be determined from equation (31). For the case of a uniform grid system $\Delta x_i = \Delta x_{i-1} = \Delta x$ and $\Delta y_j = \Delta y_{j-1} = \Delta y$, equation (31) reduces to

$$f_P = (f_P)_I + (f_P)_{II} + (f_P)_{III} + (f_P)_{IV}. \quad (32)$$

In the present investigation, a subroutine is programmed with the input $(\lambda_P, \lambda_E, \lambda_{NE}, \lambda_N)$ and the output $((f_P)_I, (f_E)_{II}, (f_{NE})_{III}, (f_N)_{IV})$. Such a technique can be easily extended to three-dimensional problems. Although additional CPU time is needed to evaluate the f-value, its achievement in providing both good accuracy and convergence rate for the solution is worth it.

Once the f-value is determined, equations (29) can be solved by using the SIS solver [6]. In this example, a solution was obtained for the parameters of $Ste = 5.2$, $\alpha_s = 1$ and $\lambda_f = 0.7692$ based on the step sizes of $\Delta x = \Delta y = 0.05$ and $\Delta \tau = 0.005$. It is important to note that, when the present results of interface fronts at various time instances are plotted in the $x(4\tau/\sigma)^{-1/2}$ vs $y(4\tau/\sigma)^{-1/2}$ coordinates, all of them are seen to coincide with each other and essentially form a single profile. This verifies the accuracy of the present numerical technique. Indeed, the interface profiles of the present problem possess a similarity solution. Figure 10 reveals a comparison between the present result with the exact solution obtained analytically by Rathjen and Jiji [20]. As in the one-dimensional problem, the present method provides a smooth profile for the two-dimensional interface. Although the present result slightly underpredicts the thickness of the solid phase, the error can be eliminated by reducing the spatial grid sizes Δx and Δy. In fact, the estimated Δf-value might have a poor accuracy when the grid sizes Δx and Δy are large and/or the time step $\Delta \tau$ is small. This could cause a numerical instability if the λ-result is very sensitive to the updated Δf-value of the pre-

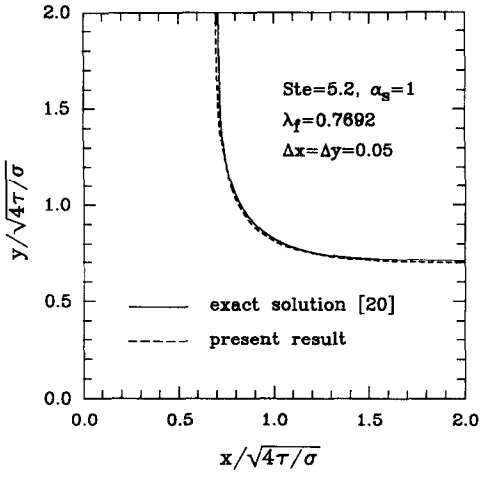

FIG. 10. The similarity profile of the liquid solid interface for a solidification phenomenon in a two-dimensional corner.

vious iteration. Fortunately, as observable from equations (29) that reducing the value of the parameter $(\Delta x)^2/\Delta\tau$ would reduce the magnitude of a_R, while the value of the weighting factor a_P is essentially maintained at $O(\alpha)$. Therefore, the sensitivity of λ on Δf can be reduced by either decreasing the spatial grid size (Δx and Δy) or increasing the time step $\Delta\tau$. Generally speaking, good numerical stability can be expected when the value of $(1-\sigma)[(\Delta x)^2+(\Delta y)^2]/\Delta\tau$ is below 0.2 for two-dimensional cases. In the present example, the value of $(1-\sigma)[(\Delta x)^2+(\Delta y)^2]/\Delta\tau$ is only 0.1613. Hence, a fast solution convergence rate was observed.

CONCLUSION

The purpose of the present work is to develop an efficient enthalpy formulation for phase change problems. As suggested by Voller, the latent heat is separated from the sensible heat. Such a treatment brings about a dependent variable (the sensible heat) that is a continuous function over the entire physical domain. Therefore, many well-developed implicit techniques such as the SIMPLE and SIMPLER algorithms [10], the weighting function scheme [16] and the SIS solver [6] can be easily implemented in the solution procedure. This is an important step in the development of the enthalpy formulation. However, like other investigators, Voller regarded the enthalpy at a grid point as the average enthalpy of the control volume containing that point. As a result, a control volume will 'suddenly' release its entire latent heat once the phase change front sweeps through its grid point. This will result in a zigzag profile for the liquid–solid interface. In addition, the definition of latent heat by Voller allows phase change to take place inside more than one control volume at the same time. To circumvent this physically impossible situation, the present formulation employs a rigorous method to evaluate the latent heat for each control volume. This strategy has been proved to have an excellent performance as demonstrated in the examples.

Along with the enthalpy model, a modified weighting function scheme is also proposed in the present study. This particular numerical scheme allows thermal conductivity (or thermal diffusivity) with discontinuities in the computational domain. In fact, the thermal diffusivity of the solid phase is much larger than that of the liquid phase for most materials. A more complex application of the present enthalpy formulation is to study the convection–conduction phase change. A subtle technique for such a problem is to regard the solid phase as a liquid with an infinite viscosity. Under such a situation, the modified weighting function scheme is expected to have a good performance in treating the viscosity jump across the interface. This will be examined in ref. [17].

Acknowledgement—The authors wish to express their appreciation to the National Science Council of the Republic of China in Taiwan for the financial support of this work through the project NSC78-0401-E007-09.

REFERENCES

1. C. Bonacina, G. Comini, A. Fasano and M. Primicerio, Numerical solution of phase-change problems, *Int. J. Heat Mass Transfer* **16**, 1825–1832 (1973).
2. N. Shamsundar and E. M. Sparrow, Analysis of multidimensional conduction phase change via the enthalpy model, *ASME J. Heat Transfer* **97**, 333–340 (1975).
3. G. E. Schneider and M. J. Raw, An implicit solution procedure for finite difference modeling of the Stefan problem, *AIAA J.* **22**, 1685–1690 (1984).
4. G. E. Schneider, Computation of heat transfer with solid/liquid phase change including free convection, *AIAA J. Thermophys. Heat Transfer* **1**, 136–145 (1987).
5. G. E. Schneider and M. Zedan, A modified strongly implicit procedure for the numerical solution of field problems, *Numer. Heat Transfer* **4**, 1–19 (1981).
6. S. L. Lee, A strongly-implicit solver for two-dimensional elliptic differential equations, *Numer. Heat Transfer* **16B**, 161–178 (1989).
7. V. R. Voller, Interpretation of the enthalpy in a discretized multidimensional region undergoing a melting/freezing phase change, *Int. Commun. Heat Mass Transfer* **10**, 323–328 (1983).
8. V. R. Voller, Implicit finite-difference solution of the enthalpy formulation of Stefan problems, *IMA J. Numer. Analysis* **5**, 201–214 (1985).
9. V. R. Voller, M. Cross and N. C. Markatos, An enthalpy method for convection/diffusion phase change, *Int. J. Numer. Meth. Engng* **24**, 271–284 (1987).
10. S. V. Patankar, *Numerical Heat Transfer and Fluid Flow*, Series in Computational Methods in Mechanics and Thermal Science. Hemisphere, New York (1980).
11. W. D. Bennon and F. P. Incropera, A continuum model for momentum, heat and species transfer in binary solid–liquid phase change systems—I. Model formulation, *Int. J. Heat Mass Transfer* **30**, 2161–2170 (1987).
12. W. D. Bennon and F. P. Incropera, A continuum model for momentum, heat and species transfer in binary solid–liquid phase change systems—II. Application to solidification in a rectangular cavity, *Int. J. Heat Mass Transfer* **30**, 2171–2187 (1987).
13. A. D. Brent, V. R. Voller and K. J. Reid, Enthalpy–porosity technique for modeling convection–diffusion

phase change: application to the melting of a pure metal, *Numer. Heat Transfer* **13**, 297–318 (1988).
14. K. H. Tacke, Discretization of the explicit enthalpy method for planar phase change, *Int. J. Numer. Meth. Engng* **21**, 543–554 (1985).
15. D. Poirier and M. Salcudean, On numerical methods used in mathematical modeling of phase change in liquid metals, *ASME J. Heat Transfer* **110**, 562–570 (1988).
16. S. L. Lee, Weighting function scheme and its application on multidimensional conservation equations, *Int. J. Heat Mass Transfer* **32**, 2065–2073 (1989).
17. W. Y. Raw and S. L. Lee, Application of weighting function scheme on convection–conduction phase change problems, *Int. J. Heat Mass Transfer* **34**, 1503–1513 (1991).
18. M. N. Ozisik, *Heat Conduction*, Chap. 10. McGraw-Hill, New York (1980).
19. N. Shamsundar and E. Rooz, Numerical methods for moving boundary problems. In *Handbook of Numerical Heat Transfer*, Chap. 18, pp. 754–755. Wiley, New York (1988).
20. K. A. Rathjen and L. M. Jiji, Heat conduction with melting or freezing in a corner, *ASME J. Heat Transfer* **93**, 101–109 (1971).

FORMULATION ENTHALPIQUE DES PROBLEMES DE CHANGEMENT DE PHASE AVEC UN GRAND SAUT DE DIFFUSIVITE A TRAVERS L'INTERFACE

Résumé—On propose une formulation enthalpique pour un matériau à changement de phase (PCM) ayant une température distincte de solidification. La chaleur latente est séparée de la chaleur sensible de façon qu'il existe une variable dépendante (la chaleur sensible) qui est une fonction continue dans tout le domaine physique. Dans chaque volume de contrôle, la chaleur latente est rigoureusement évaluée à partir de la fraction de phase liquide pour décrire une évolution de chaleur latente. Dans la transformation sans dimension, le temps caractéristique est défini en fonction du nombre de Stefan. Les coefficients des termes variables sont ainsi toujours inférieurs à l'unité. Ceci donne une bonne stabilité numérique pour un nombre de Stefan quelconque. De plus cette transformation particulière rend la formulation enthalpique applicable aux problèmes à une seule phase si on assigne un nombre de Stefan infini. Pour tenir compte du saut de diffusivité thermique à l'interface liquide–solide, on développe un schéma à fonction de pondération. A travers quelques exemples, la présente formulation enthalpique produit un interface précis et lisse pour un PCM ayant un point de congélation distinct.

BESCHREIBUNG VON PHASENWECHSELPROBLEMEN MIT HILFE DER ENTHALPIE FÜR DEN FALL STARK UNTERSCHIEDLICHER TEMPERATURLEITFÄHIGKEITEN BEIDERSEITS DER GRENZFLÄCHE

Zusammenfassung—Die Vorgänge in einem schmelzbaren Material (PCM) mit eindeutiger Verfestigungstemperatur werden unter Verwendung der Enthalpie beschrieben. Die latente und die fühlbare Wärme werden so separiert, daß sich eine abhängige Variable (die fühlbare Wärme) als kontinuierliche Funktion im gesamten betrachteten Gebiet ergibt. In jedem Kontrollvolumen wird aufgrund des Anteils der flüssigen Phase die latente Wärme berechnet. Für die dimensionslose Transformation wird mit Hilfe der Stefan-Zahl die charakteristische Zeit definiert. Die Koeffizienten der instationären Terme werden auf diese Weise stets kleiner als 1. Daraus resultiert für jede Stefan-Zahl eine gute numerische Stabilität. Außerdem ermöglicht diese spezielle Transformation die Anwendung des vorgestellten Enthalpie-Verfahrens auf Probleme ohne Phasenänderung, wenn die Stefan-Zahl als unendlich groß angenommen wird. Zur Berücksichtigung einer sprungförmigen Änderung der Temperaturleitfähigkeit an der flüssig/festen Phasengrenzfläche werden modifizierte Gewichtungsfunktionen entwickelt. Anhand einiger Beispiele zeigt sich, daß das vorgestellte Verfahren einen genauen und glatten Verlauf der flüssig/festen Grenzfläche für schmelzbare Materialien mit einem bestimmten Verfestigungspunkt liefert.

ПРЕДСТАВЛЕНИЕ ЭНТАЛЬПИИ ДЛЯ ЗАДАЧ ФАЗОВОГО ПЕРЕХОДА С БОЛЬШИМ СКАЧКОМ ТЕМПЕРАТУРОПРОВОДНОСТИ НА ГРАНИЦЕ РАЗДЕЛА

Аннотация—Предложено представление энтальпии для материала с фазовым переходом и резко выраженной температурой замерзания. Скрытая теплота при этом отделена от теплосодержания, что привело к существованию зависимой переменной (теплосодержание), являющейся непрерывной функцией во всей физической области. В каждом контрольном объеме по доле жидкой фазы строго определена теплота для достижения ее равномерной эволюции. При безразмерном преобразовании характерное время выражено через число Стефана. Таким образом, коэффициенты нестационарных слагаемых всегда составляют меньше единицы, что позволяет достигнуть хорошую численную устойчивость при любом значении числа Стефана. Кроме того, указанное преобразование позволяет применять предложенное представление энтальпии к однофазным задачам, если задано бесконечное число Стефана. Для учета скачка температуропроводности на границе раздела жидкость–твердое тело разработана модифицированная схема весовых функций. На нескольких примерах показано, что данное представление энтальпии позволяет точно определить гладкую границу раздела жидкость–твердое тело для материалов с фазовым переходом, имеющих резко выраженную точку замерзания.